

## Line-Graph Approach to Spiral Spin Liquids


Shang Gao,<sup>1,2,\*†</sup> Ganesh Pokharel,<sup>2,3</sup> Andrew F. May,<sup>2</sup> Joseph A. M. Paddison,<sup>2</sup> Chris Pasco,<sup>2</sup> Yaohua Liu,<sup>1</sup> Keith M. Taddei,<sup>1</sup> Stuart Calder,<sup>1</sup> David G. Mandrus,<sup>2,3,4</sup> Matthew B. Stone,<sup>1</sup> and Andrew D. Christianson<sup>2</sup>

<sup>1</sup>Neutron Scattering Division, Oak Ridge National Laboratory, Oak Ridge, Tennessee 37831, USA

<sup>2</sup>Materials Science & Technology Division, Oak Ridge National Laboratory, Oak Ridge, Tennessee 37831, USA

<sup>3</sup>Department of Physics & Astronomy, University of Tennessee, Knoxville, Tennessee 37996, USA

<sup>4</sup>Department of Materials Science & Engineering, University of Tennessee, Knoxville, Tennessee 37996, USA

 (Received 2 June 2022; revised 20 September 2022; accepted 20 October 2022; published 29 November 2022)

Competition among exchange interactions is able to induce novel spin correlations on a bipartite lattice without geometrical frustration. A prototype example is the spiral spin liquid, which is a correlated paramagnetic state characterized by subdimensional degenerate propagation vectors. Here, using spectral graph theory, we show that spiral spin liquids on a bipartite lattice can be approximated by a further-neighbor model on the corresponding line-graph lattice that is nonbipartite, thus broadening the space of candidate materials that may support the spiral spin liquid phases. As illustrations, we examine neutron scattering experiments performed on two spinel compounds,  $\text{ZnCr}_2\text{Se}_4$  and  $\text{CuInCr}_4\text{Se}_8$ , to demonstrate the feasibility of this new approach and expose its possible limitations in experimental realizations.

DOI: [10.1103/PhysRevLett.129.237202](https://doi.org/10.1103/PhysRevLett.129.237202)

**Introduction.**—A spiral spin liquid (SSL) is an exotic correlated paramagnetic state of “subdimensional” degeneracy, meaning that the propagation vectors  $\mathbf{q}$  of the ground states form a continuous manifold, or spiral surface, in a dimension that is reduced from the original system [1–14]. Similar to geometrically frustrated magnets [15,16], a SSL may host topological spin textures [17–19] and quantum spin liquid states [3–5,20–22]. What differentiates a SSL from a conventional frustrated magnet is the subdimensional degeneracy, which induces highly distinctive dynamics since the spins are confined to fluctuate collectively as nonlocal spirals [23]. Recent calculations on a square lattice reveal that the low-energy fluctuations in a SSL may behave as topological vortices in momentum space [23], leading to an effective tensor gauge theory with unconventional fracton quadrupole excitations that are deeply connected to theories of quantum information, elasticity, and gravity [24–29].

To date, bipartite lattices have been the primary avenue through which SSLs are studied. This is because the ground state degeneracy on a bipartite lattice can be exact, so that all spin spirals with  $\mathbf{q}$  over the spiral surface have exactly the same energy [5]. Although this degeneracy stabilizes the SSL down to very low temperatures [1,3], it also imposes a strong constraint on real materials because most of the known bipartite-lattice compounds are dominated by the nearest-neighbor (NN) interactions  $J_1$  [30–44]. Even for the established model compounds where the second-neighbor interactions  $J_2$  are relatively strong [17,45,46], the degeneracy over the spiral surface is only approximate due to the existence of further perturbations [14]. This degeneracy lifting results in an approximate SSL state at

elevated temperatures where thermal fluctuations overcome the slight energy difference among the spirals.

Inspired by recent density-functional theory calculations for the breathing pyrochlore lattice compounds [47], here we seek the realization of an approximate SSL, i.e., a SSL with an approximate degeneracy, beyond the bipartite lattices. According to the Luttinger-Tisza theory [48,49], the degeneracy of a SSL model is encoded in the minimum manifold of the interaction matrix. Using graph theory [50,51], we show that the  $J_1$ - $J_2$  model on a bipartite lattice shares the same minimum manifold with a  $J_1$ - $J_3$  model on the corresponding line-graph lattice, where  $J_3$  denotes the third-neighbor interaction. Thus, an approximate SSL state is achieved in the latter case when  $J_3$  is sufficiently strong, which greatly expands the range of materials that may support a SSL state. This line-graph approach to SSL is vetted through neutron scattering experiments performed on two Cr-based chalcogenide spinels:  $\text{ZnCr}_2\text{Se}_4$  and  $\text{CuInCr}_4\text{Se}_8$ .

**Line-graph approach.**—Our starting point is a Heisenberg model on a  $l$ -regular lattice, where  $l$  counts the number of the NN sites. In the presence of a uniform NN exchange interaction  $J_1$ , the coupled spins form a undirected graph  $G = (V, D)$ , with  $V$  denoting the set of vertices (i.e., the spin sites) and  $D$  denoting the set of edges (i.e., the NN bonds). Two vertices  $i$  and  $j$  are called “adjacent” if the graph contains an edge  $e = \{i, j\}$ , and the adjacency matrix is defined as  $A(G)_{ij} = 1$  for  $\{i, j\} \in D$  and 0 otherwise. Following this definition, the spin Hamiltonian,  $\mathcal{H} = J_1 \sum_{\langle ij \rangle} \mathbf{S}_i \cdot \mathbf{S}_j$  with  $\langle ij \rangle$  denoting the NN bonds, can be expressed through the adjacency matrix as  $\mathcal{H} = \frac{1}{2} J_1 A(G)_{ij} \mathbf{S}_i \cdot \mathbf{S}_j$ . Therefore, according to the

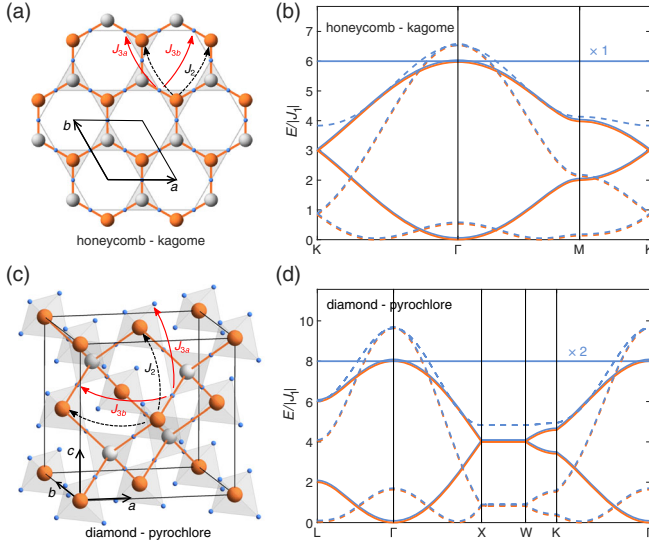


FIG. 1. (a) The line graph of a bipartite honeycomb lattice (large spheres linked by orange bonds) is a kagome lattice (small spheres linked by gray bonds).  $J_1$  is the nearest-neighbor exchange coupling. Black dashed (red solid) arrows indicate the second-neighbor coupling  $J_2$  (third-neighbor couplings  $J_{3a}$  and  $J_{3b}$ ) over the honeycomb (kagome) lattice. (b) Eigenbands of the interaction matrix of Heisenberg models on the honeycomb and kagome lattices. Orange solid (dashed) lines are the two eigenbands for the  $J_1$  model ( $J_1$ - $J_2$  model with  $J_2/J_1 = -0.25$ ) on the honeycomb lattice, which overlap with the two lower eigenbands of the  $J_1$  model ( $J_1$ - $J_3$  model with  $J_3/J_1 = -0.25$ ) on the kagome lattice shown in blue solid (dashed) lines. (c),(d) Similar correspondence exists between the diamond and pyrochlore lattices. The interaction matrices for the  $J_1$  model ( $J_1$ - $J_2$  model with  $J_2/J_1 = -0.3$ ) on the diamond lattice and the  $J_1$  model ( $J_1$ - $J_3$  model with  $J_3/J_1 = -0.3$ ) on the pyrochlore lattice share two same eigenbands shown by the overlapping orange and blue solid (dashed) lines.

Luttinger-Tisza theory [1,5], the classical ground state of  $\mathcal{H}$  can be determined from the eigensolution of  $A(G)$ , of which the eigenvalues are defined as the “spectrum” of the graph, denoted as  $\sigma(G)$ .

Algebraic graph theory indicates that related graphs should have related spectra [50,51]. Of interest here is the line graph  $L_G$  [52,53], whose vertices correspond to the edges of the root graph  $G$  and are adjacent if the original edges share a vertex:  $L_G = (D, \{\{e, e'\} | e \cup e' \neq \emptyset, e \neq e'\})$ . For a regular bipartite graph  $G$ , a convenient way to define its line graph is to select the vertices at the midpoints of the original edges. As illustrated in Fig. 1, for the honeycomb ( $l = 3$ ) and diamond ( $l = 4$ ) lattices that are the prototype hosts of the SSL, their line graphs form the kagome and pyrochlore lattices, respectively. According to graph theory [50,51], the spectra of  $G$  and  $L_G$  are related by

$$\sigma(L_G) = (-2)^{m-n} \cup \sigma(G) + l - 2, \quad (1)$$

where  $m$  ( $n$ ) is the total number of edges (vertices) of the root graph  $G$ . In reciprocal space, Eq. (1) indicates the existence of flat eigenbands on  $L_G$  with a degeneracy of  $l - 2$ , which has been the focus of many recent studies [51,54–56]. More importantly, it reveals that the nonflat eigenbands of  $\sigma(L_G)$  and  $\sigma(G)$  share the same dispersion up to a constant of  $l - 2$ , and their eigenvectors are related by the incident matrix as discussed in Ref. [57].

Such a spectrum correspondence can be immediately verified for Heisenberg models. On a regular lattice of  $g$  sublattices and  $N$  primitive cells, the interaction matrix of a  $J_1$ -only model

$$\mathcal{J}_1^{\alpha\beta}(\mathbf{q}) = \frac{J_1}{N} \sum_{\substack{i \in \alpha, j \in \beta \\ ij \in \langle ij \rangle}} \exp[-i\mathbf{q} \cdot (\mathbf{r}_i - \mathbf{r}_j)] \quad (2)$$

is a  $g \times g$  hollow matrix with zero diagonal elements. The eigenbands  $\nu(\mathbf{q})$  for  $J_1 < 0$  are shown as solid lines in Fig. 1(b) for the honeycomb and kagome lattices, and in Fig. 1(d) for the diamond and pyrochlore lattices. The minimum of the eigenbands  $\nu_{\min}$  has been subtracted for comparison. Analytical expressions for the eigenbands are presented in the Supplemental Material [58]. Aside from the top flat bands in blue color, the two dispersive bands  $\nu_{\pm}(\mathbf{q}) - \nu_{\min}$  on the kagome (pyrochlore) lattice overlap exactly with those on the honeycomb (diamond) lattice, which is a direct consequence of spectral graph theory.

This eigenband correspondence is maintained under the addition of certain further-neighbor interactions. For the  $J_1$ - $J_2$  model on a bipartite lattice,  $J_2$  couples the spins of the same sublattices. Therefore, its contribution to  $\mathcal{J}(\mathbf{q})$  is a diagonal matrix  $\mathcal{J}_2(\mathbf{q})$  that commutes with  $\mathcal{J}_1(\mathbf{q})$ , leading to a  $\mathbf{q}$ -dependent shift  $\gamma_G(\mathbf{q})$  of the eigenbands with  $\gamma_G(\mathbf{q}) = (J_2/Ng) \sum_{ij \in \langle\langle ij \rangle\rangle} \exp[-i\mathbf{q} \cdot (\mathbf{r}_i - \mathbf{r}_j)]$ , where  $\langle\langle ij \rangle\rangle$  are the second-neighbor bonds [58]. Similar conclusions can be drawn for the  $J_1$ - $J_3$  model on the line-graph lattices, as  $J_3$  (including both  $J_{3a}$  and  $J_{3b}$ ) also couples spins of the same sublattices [58]. Since  $J_2(G)$  on the root-graph lattice and  $J_3(L_G)$  on the line-graph lattice share the same exchange paths as compared in Figs. 1(a) and 1(c), we expect, in the case of  $J_2(G) = J_3(L_G)$ , the same dispersive eigenbands up to a constant on the root- and line-graph lattices. This correspondence is illustrated by the dashed lines in Figs. 1(b) and 1(d).

*Approximate SSL.*—An approximate SSL can be realized on the line-graph lattices through the eigenband correspondence. Following the results of the  $J_1$ - $J_2$  model on the bipartite lattices [1,5], it is clear that for the  $J_1$ - $J_3$  model on a line-graph lattice the eigenband minima of  $\mathcal{J}(\mathbf{q})$  will form a degenerate manifold in reciprocal space at  $|J_3/J_1| > 1/(2l)$ , where  $l$  is the number of the NN sites on the root-graph lattice. Here,  $J_1$  and  $J_3$  should be ferromagnetic and antiferromagnetic, respectively, as the additional flat bands on line graphs remove the ferromagnetic-antiferromagnetic duality of a bipartite lattice. Since the

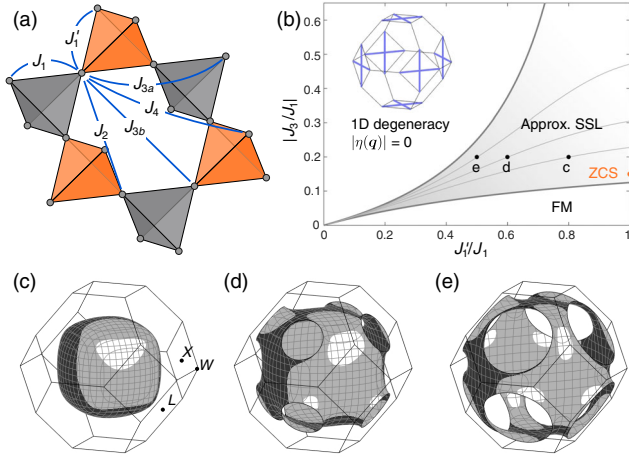


FIG. 2. (a) The breathing pyrochlore lattice is composed of corner-sharing tetrahedra of two different sizes, which results in alternating  $J_1$  and  $J'_1$  couplings over the gray and orange tetrahedra, respectively. The exchange paths of the  $J_2$ ,  $J_{3a}$ ,  $J_{3b}$ , and  $J_4$  interactions are also indicated. (b) Phase diagram on the breathing pyrochlore lattice with ferromagnetic  $J_1$  and  $J'_1$  interactions together with antiferromagnetic  $J_3$  interactions assuming  $J_{3a} = J_{3b}$ . The shaded area indicates the region where an approximate SSL phase can be stabilized by thermal fluctuations. Contour lines for constant  $|\eta(\mathbf{q})|$  are shown in the approximate SSL phase. Along these lines, the spiral surface stays the same. Location of  $\text{ZnCr}_2\text{Se}_4$  (ZCS) with  $J_1 = J'_1$  and  $|J_3/J_1| = 0.15$  is indicated by the yellow dot. Inset shows the degenerate manifold (blue lines) for  $4J_3 > J_1 J'_1 / |J_1 - J'_1|$  out of the SSL regime. (c)–(e) Characteristic spiral surfaces with quasidegenerate energies in the first Brillouin zone at  $|J_3/J_1| = 0.2$  and  $J'_1/J_1 = 0.8$  (c),  $0.6$  (d), and  $0.5$  (e). These points are indicated on the phase diagram in (b) using the panel labels.

equal moment constraint over the eigenvectors of  $\mathcal{J}(\mathbf{q})$  is not always satisfied for  $\mathbf{q}$  over the minimum manifold [58], the SSL realized through the line-graph approach is approximate and needs to be stabilized by thermal fluctuations. As discussed in the Supplemental Material [58], the degeneracy breaking over the spiral surface is relatively weak, which contrasts with the strong modulation in the previously studied half-moon patterns [57,71–73]. This weak degeneracy breaking on the line-graph lattices leads to a stable SSL state in a wide temperature regime that is comparable to that on the bipartite lattices.

Before making comparisons to the experimental data, we further generalize the SSL model by incorporating a breathing distortion on the line-graph lattice so that the NN interactions are modulated alternately as  $J_1$  and  $J'_1$  [47,74,75]. For the breathing pyrochlore lattice shown in Fig. 2(a), the eigenbands of  $\mathcal{J}(\mathbf{q})$  can be solved as follows [58]:

$$\begin{aligned} \nu_{1,2} &= J_3 \kappa(\mathbf{q}) \pm \sqrt{4(J_1 - J'_1)^2 + J_1 J'_1 |\eta(\mathbf{q})|^2 + (J_1 + J'_1)}, \\ \nu_{3,4} &= J_3 \kappa(\mathbf{q}) - (J_1 + J'_1), \end{aligned}$$

where  $\eta(\mathbf{q}) = \sum_{n=1}^4 \exp(-i\mathbf{q} \cdot \mathbf{d}_n)$  with  $\mathbf{d}_n$  denoting the four bonding vectors around each spin site [58] and  $\kappa(\mathbf{q}) = |\eta(\mathbf{q})|^2 - 4$ . Assuming  $J_1 < J'_1 < 0$  and  $J_3 > 0$ , an approximate SSL state is realized for  $J_1 J'_1 / |J_1 + J'_1| < 4J_3 < J_1 J'_1 / |J_1 - J'_1|$ . The corresponding phase diagram is presented in Fig. 2(b). Representative spiral surfaces in the approximate SSL phase at  $|J_3/J_1| = 0.2$  are shown in Figs. 2(c)–2(e) for  $J'_1/J_1 = 0.8, 0.6$ , and  $0.5$ , respectively. The surfaces are identical to those on the diamond lattice [1]. Similar conclusions on the breathing kagome lattice are presented in the Supplemental Material [58].

**ZnCr<sub>2</sub>Se<sub>4</sub> with a regular pyrochlore lattice.**—The Cr-based chalcogenide spinels present nearly ideal model compounds to demonstrate the proposed line-graph approach to SSLs. In these systems,  $J_1$  is ferromagnetic due to the  $90^\circ$  superexchange path, while  $J_2 \sim 0$  due to negligible orbital overlap [76,77]. As the first example, we study the short-range spin correlations in  $\text{ZnCr}_2\text{Se}_4$ , where the  $\text{Cr}^{3+}$  ( $S = 3/2$ ) ions form a regular pyrochlore lattice.

Single crystals of  $\text{ZnCr}_2\text{Se}_4$  were grown using the chemical vapor transport method [58]. Figure 3 summarizes the diffuse neutron scattering results measured on CORELLI at the Spallation Neutron Source (SNS), Oak Ridge National Laboratory (ORNL) [58]. With the statistical chopper, the elastic channel of our CORELLI data has an average energy resolution of about 0.8 meV for an incident neutron energy range of 13 to 33 meV. At 20 K, below the Néel transition temperature  $T_N \sim 22$  K, magnetic Bragg peaks indexed by  $\mathbf{q} = (0, 0, 0.47)$  are observed [see Fig. 3(a)]. This is consistent with the helical ground state reported previously [78–80], with the weak ringlike scattering mainly arising from the low-energy magnon excitations [77,81]. At 30 K, above  $T_N$ , magnetic Bragg peaks are replaced by broad diffuse scattering with a spherical shape [see Figs. 3(b)–3(d)], evidencing the emergence of an approximate SSL state where gapped excitations are replaced by quasielastic fluctuations [58].

Assuming a Heisenberg model with exchange interactions up to the fourth neighbors ( $J_4$ ), we fit the diffuse scattering data using the self-consistent Gaussian approximation method [58]. The calculated slices in Figs. 3(b)–3(d) reproduce the experimental data. The coupling strengths are fitted as  $J_1 = -2.86(8)$ ,  $J_2 = 0.00(1)$ ,  $J_3 = 0.48(1)$ , and  $J_4 = -0.057(1)$  meV, which is very close to the values determined by inelastic neutron scattering (INS) [77,81] and indicates marginal changes in the coupling strengths across the phase transition. The weak strengths of the  $J_2$  and  $J_4$  interactions allow a direct verification of the line-graph approach that is based on a  $J_1$ - $J_3$  model. The solid circles on top of the calculated patterns in Figs. 3(b)–3(d) are the contours of the spiral surface predicted by the  $J_1$ - $J_3$  model with  $J_3/J_1 = -0.15$ . The contours capture the shapes of the diffuse scattering patterns. As compared in the Supplemental Material [58], the existence of the

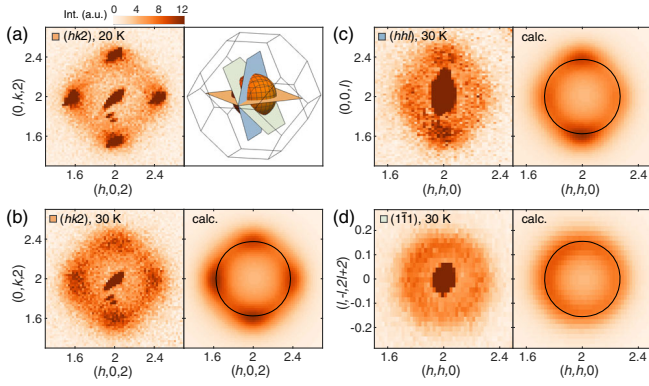


FIG. 3. Quasistatic spin correlations in  $\text{ZnCr}_2\text{Se}_4$  measured on CORELLI at (a) 20 K and (b)–(d) 30 K. Slices are along the  $(hk2)$  plane in panels (a),(b),  $(hhl)$  plane in panel (c), and  $(\bar{1}\bar{1}1)$  plane in panel (d). The right subpanel in (a) shows the complete spiral surface for the  $J_1$ - $J_3$  model on a pyrochlore lattice with  $J_3/J_1 = -0.15$ . The flat planes correspond to the slice directions as indicated by the colored plaquette at the top left corner in each panel. The right subpanels in (b)–(d) are the calculated diffuse scattering patterns for the fitted  $J_1$ - $J_2$ - $J_3$ - $J_4$  model. Solid line is the spiral surface predicted by the  $J_1$ - $J_3$  model with  $J_3/J_1 = -0.15$ . The same linear intensity scale is employed in all panels.

ferromagnetic  $J_4$  interaction slightly reduces the radius of the spiral surface while strongly modulating the scattering intensities.

**CuInCr<sub>4</sub>Se<sub>8</sub> with a breathing pyrochlore lattice.**—Until now, we have assumed a uniform  $J_3$  interaction. In real materials, the  $J_3$  exchange paths on a line-graph lattice can be different as indicated in Fig. 1. This may lead to different coupling strengths and destabilize the SSL state. As the second example, we study the spin correlations in the breathing pyrochlore lattice compound  $\text{CuInCr}_4\text{Se}_8$  [82], which has been proposed as a SSL candidate from density-functional theory calculations [47].

A polycrystalline sample of  $\text{CuInCr}_4\text{Se}_8$  was synthesized through the solid state reaction method [58]. INS experiments were performed on SEQUOIA at the SNS, ORNL. Neutron diffraction experiments were performed on HB-2A at the High Flux Isotope Reactor (HFIR), ORNL. As is consistent with the previous report [82], magnetic susceptibility shown in Fig. 4(a) suggests a spin glasslike transition at  $T_f \sim 15$  K with a clear frequency dependence. This is confirmed in the neutron diffraction results presented in Fig. 4(b), where only broad magnetic features are observed down to 0.25 K. The weak features at  $Q \sim 0.41$  and  $0.72 \text{ \AA}^{-1}$  can be indexed by  $\mathbf{q} = (0.48, 0.48, 0)$ , while their intensities exhibit a history dependence as expected for a spin glass state.

Figures 4(c)–4(e) present the equal-time spin correlations obtained by integrating the INS spectra from  $[-20, 20]$  meV [58]. Assuming a  $J_1$ - $J'_1$ - $J_{3a}$ - $J_{3b}$  Heisenberg spin model, we fit the diffuse scattering data by the self-consistent Gaussian

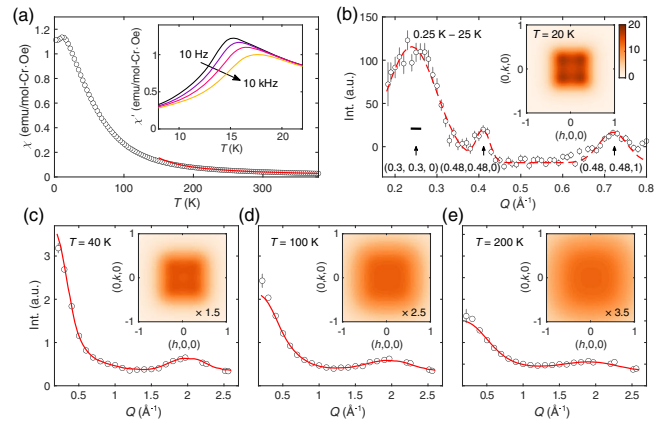


FIG. 4. (a) dc magnetic susceptibility of  $\text{CuInCr}_4\text{Se}_8$  measured in a  $1 \times 10^4$  Oe field (circles). Red line shows the Curie Weiss fit at temperatures between 200 and 380 K. The fitted magnetic moment and Weiss temperature are  $\mu_{\text{eff}} = 4.6 \mu_B/\text{Cr}$  and 97(2) K, respectively. The inset shows the frequency dependence of the real part of the ac susceptibility measured in a 10 Oe field. Imaginary part of the ac susceptibility is presented in the Supplemental Material [58]. (b) Difference between the neutron diffraction intensity at 0.25 and 25 K measured on HB-2A. The dashed line is a guide to the eyes. Positions of the characteristic wave vectors are indicated by arrows. The full width at half maximum (FWHM) of the closest nuclear reflection is indicated by the horizontal bar. Inset shows the calculated neutron diffuse scattering pattern in the  $(h, k, 0)$  plane at  $T = 20$  K for  $J_{3a} = 0.07$  meV (see text). (c)–(e) Circles show the  $Q$  dependence of the equal-time spin correlations at  $T = 40$  (c), 100 (d), and 200 K (e). Results of the self-consistent Gaussian approximation fits using the  $J_1$ - $J'_1$ - $J_{3a}$ - $J_{3b}$  model are shown by the red solid lines. Insets are the calculated neutron diffuse scattering patterns in the  $(h, k, 0)$  plane for  $J_{3a} = 0.07$  meV at the corresponding temperatures (see text).

approximation method [58,83]. The fitted results are shown in Figs. 4(c)–4(e) as solid lines. The fitted coupling strengths are  $J_1 = -1.6(2)$ ,  $J'_1 = -5.4(3)$ ,  $J_{3a} = 0.1(1)$ , and  $J_{3b} = 0.6(1)$  meV, where the different strengths for  $J_{3a}$  and  $J_{3b}$  are necessary for a satisfactory fit. As shown in the inset of Figs. 4(b)–4(e), the spin correlations in the  $(hk0)$  plane do not follow a circular shape, implying the absence of a SSL state due to the unequal  $J_{3a}$  and  $J_{3b}$  interactions.

The fitted parameter set provides an explanation for the glassy ground state in  $\text{CuInCr}_4\text{Se}_8$ .  $J_{3a}$ , being the weakest interaction in the  $J_1$ - $J'_1$ - $J_{3a}$ - $J_{3b}$  model, is however the most crucial parameter in determining the exact length of the long-range order  $\mathbf{q} = (q, q, 0)$ . Within the standard deviation of  $J_{3a}$ ,  $q$  varies from 0 at  $J_{3a} = 0$  up to  $\sim 0.4$  at  $J_{3a} = 0.2$  meV. Therefore, the broad diffuse scattering at  $Q \sim 0.25 \text{ \AA}^{-1}$ , which is tentatively indexed as  $(0.3, 0.3, 0)$  in Fig. 4(b), may arise from a finite distribution in  $J_{3a}$  due to a tiny amount of structural defects. Weaker features indexed by  $\mathbf{q} = (0.48, 0.48, 0)$  may be stabilized by local structural distortions considering its proximity to the commensurate  $(\frac{1}{2}, \frac{1}{2}, 0)$  position [84,85]. Studies of a single crystal sample will help verify the proposed mechanism.

*Conclusion.*—We have presented a line-graph approach to achieve approximate SSLs on nonbipartite lattices, which allows the experimental exploration of SSLs in a broader family of compounds. Besides  $\text{ZnCr}_2\text{Se}_4$  studied in this Letter, chalcogenide spinels like  $\text{ZnCr}_2\text{S}_4$  [79] and  $\text{HgCr}_2\text{S}_4$  [86] are worth further investigations as an incommensurate helical ground state has been observed. The approximate SSLs on the line-graph lattices also provide a new platform to explore field-induced topological spin textures since the helicity of the single- $q$  component is maintained [18]. Such a mechanism may account for the magnetic skyrmions in the breathing kagome-lattice compound  $\text{Gd}_3\text{Ru}_4\text{Al}_{12}$  [74]. On the theoretical side, it remains an open question whether the approximate SSLs may evolve into quantum spin liquids under sufficient quantum fluctuations. It is also interesting to explore whether the fracton physics predicted for the exact SSLs [23] may survive to some extent in the approximate SSLs.

We acknowledge helpful discussions with Jyong-Hao Chen. This work was supported by the U.S. Department of Energy, Office of Science, Basic Energy Sciences, Materials Sciences and Engineering Division. This research used resources at the Spallation Neutron Source (SNS) and the High Flux Isotope Reactor (HFIR); both are DOE Office of Science User Facilities operated by the Oak Ridge National Laboratory (ORNL). G. P. acknowledges support from the Gordon and Betty Moore Foundation's EPIQS Initiative, Grant No. GBMF9069.

\*Corresponding author.

sgao.physics@gmail.com

<sup>†</sup>Present address: Department of Physics, University of Science and Technology of China, Hefei, 230026 Anhui, China.

- [1] D. Bergman, J. Alicea, E. Gull, S. Trebst, and L. Balents, *Nat. Phys.* **3**, 487 (2007).
- [2] S. B. Lee and L. Balents, *Phys. Rev. B* **78**, 144417 (2008).
- [3] A. Mulder, R. Ganesh, L. Capriotti, and A. Paramekanti, *Phys. Rev. B* **81**, 214419 (2010).
- [4] H. Zhang and C. A. Lamas, *Phys. Rev. B* **87**, 024415 (2013).
- [5] N. Niggemann, M. Hering, and J. Reuther, *J. Phys. Condens. Matter* **32**, 024001 (2020).
- [6] J. Attig and S. Trebst, *Phys. Rev. B* **96**, 085145 (2017).
- [7] P. Balla, Y. Iqbal, and K. Penc, *Phys. Rev. Res.* **2**, 043278 (2020).
- [8] P. Balla, Y. Iqbal, and K. Penc, *Phys. Rev. B* **100**, 140402(R) (2019).
- [9] G. Chen, *Phys. Rev. B* **96**, 020412(R) (2017).
- [10] X.-P. Yao, J. Q. Liu, C.-J. Huang, X. Wang, and G. Chen, *Front. Phys.* **16**, 53303 (2021).
- [11] C.-J. Huang, J. Q. Liu, and G. Chen, *Phys. Rev. Res.* **4**, 013121 (2022).
- [12] F. L. Buessen, M. Hering, J. Reuther, and S. Trebst, *Phys. Rev. Lett.* **120**, 057201 (2018).
- [13] J. Q. Liu, F.-Y. Li, G. Chen, and Z. Wang, *Phys. Rev. Res.* **2**, 033260 (2020).
- [14] Y. Iqbal, T. Müller, H. O. Jeschke, R. Thomale, and J. Reuther, *Phys. Rev. B* **98**, 064427 (2018).
- [15] S. T. Bramwell and M. J. P. Gingras, *Science* **294**, 1495 (2001).
- [16] L. Balents, *Nature (London)* **464**, 199 (2010).
- [17] S. Gao, O. Zaharko, V. Tsurkan, Y. Su, J. S. White, G. S. Tucker, B. Roessli, F. Bourdarot, R. Sibille, D. Chernyshov, T. Fennell, A. Loidl, and C. Rüegg, *Nat. Phys.* **13**, 157 (2017).
- [18] S. Gao, H. D. Rosales, F. A. Gómez Albarracín, V. Tsurkan, G. Kaur, T. Fennell, P. Steffens, M. Boehm, P. Čermák, A. Schneidewind, E. Ressouche, D. C. Cabra, C. Rüegg, and O. Zaharko, *Nature (London)* **586**, 37 (2020).
- [19] T. Shimokawa, T. Okubo, and H. Kawamura, *Phys. Rev. B* **100**, 224404 (2019).
- [20] C. Balz, B. Lake, J. Reuther, H. Luetkens, R. Schonemann, T. Herrmannsdorfer, Y. Singh, A. T. M. Nazmul Islam, E. M. Wheeler, J. A. Rodriguez-Rivera, T. Guidi, G. G. Simeoni, C. Baines, and H. Ryll, *Nat. Phys.* **12**, 942 (2016).
- [21] S. Biswas and K. Damle, *Phys. Rev. B* **97**, 115102 (2018).
- [22] R. Pohle, H. Yan, and N. Shannon, *Phys. Rev. B* **104**, 024426 (2021).
- [23] H. Yan and J. Reuther, *Phys. Rev. Res.* **4**, 023175 (2022).
- [24] M. Pretko, *Phys. Rev. B* **95**, 115139 (2017).
- [25] M. Pretko, *Phys. Rev. D* **96**, 024051 (2017).
- [26] M. Pretko and L. Radzihovsky, *Phys. Rev. Lett.* **120**, 195301 (2018).
- [27] H. Yan, *Phys. Rev. B* **99**, 155126 (2019).
- [28] R. M. Nandkishore and M. Hermele, *Annu. Rev. Condens. Matter Phys.* **10**, 295 (2019).
- [29] M. Pretko, X. Chen, and Y. You, *Int. J. Mod. Phys. A* **35**, 2030003 (2020).
- [30] N. Tristan, J. Hemberger, A. Krimmel, H.-A. Krug von Nidda, V. Tsurkan, and A. Loidl, *Phys. Rev. B* **72**, 174404 (2005).
- [31] T. Suzuki and H. Nagai and M. Nohara and H. Takagi, *J. Phys. Condens. Matter* **19**, 145265 (2007).
- [32] A. Krimmel, H. Mutka, M. M. Koza, V. Tsurkan, and A. Loidl, *Phys. Rev. B* **79**, 134406 (2009).
- [33] M. Matsuda, M. Azuma, M. Tokunaga, Y. Shimakawa, and N. Kumada, *Phys. Rev. Lett.* **105**, 187201 (2010).
- [34] G. J. MacDougall, D. Gout, J. L. Zarestky, G. Ehlers, A. Podlesnyak, M. A. McGuire, D. Mandrus, and S. E. Nagler, *Proc. Natl. Acad. Sci. U.S.A.* **108**, 15693 (2011).
- [35] O. Zaharko, N. B. Christensen, A. Cervellino, V. Tsurkan, A. Maljuk, U. Stuhr, C. Niedermayer, F. Yokaichiya, D. N. Argyriou, M. Boehm, and A. Loidl, *Phys. Rev. B* **84**, 094403 (2011).
- [36] H. S. Nair, Z. Fu, J. Voigt, Y. X. Su, and T. Brückel, *Phys. Rev. B* **89**, 174431 (2014).
- [37] G. J. MacDougall, A. A. Aczel, Y. Su, W. Schweika, E. Faulhaber, A. Schneidewind, A. D. Christianson, J. L. Zarestky, H. D. Zhou, D. Mandrus, and S. E. Nagler, *Phys. Rev. B* **94**, 184422 (2016).
- [38] L. Ge, J. Flynn, J. A. M. Paddison, M. B. Stone, S. Calder, M. A. Subramanian, A. P. Ramirez, and M. Mourigal, *Phys. Rev. B* **96**, 064413 (2017).
- [39] J. R. Chamorro, L. Ge, J. Flynn, M. A. Subramanian, M. Mourigal, and T. M. McQueen, *Phys. Rev. Mater.* **2**, 034404 (2018).
- [40] V. Tsurkan, H.-A. Krug von Nidda, J. Deisenhofer, P. Lunkenheimer, and A. Loidl, *Phys. Rep.* **926**, 1 (2021).

- [41] Y. Haraguchi, K. Nawa, C. Michioka, H. Ueda, A. Matsuo, K. Kindo, M. Avdeev, T. J. Sato, and K. Yoshimura, *Phys. Rev. Mater.* **3**, 124406 (2019).
- [42] A. H. Abdeldaim, T. Li, L. Farrar, A. A. Tsirlin, W. Yao, A. S. Gibbs, P. Manuel, P. Lightfoot, G. J. Nilsen, and L. Clark, *Phys. Rev. Mater.* **4**, 104414 (2020).
- [43] A. Otsuka, Y. Shimizu, G. Saito, M. Maesato, A. Kiswandhi, T. Hiramatsu, Y. Yoshida, H. Yamochi, M. Tsuchiizu, Y. Nakamura, H. Kishida, and H. Ito, *Bull. Chem. Soc. Jpn.* **93**, 260 (2020).
- [44] C. Wessler, B. Roessli, K. W. Krämer, B. Delley, O. Waldmann, L. Keller, D. Cheptiakov, H. B. Braun, and M. Kenzelmann, *npj Quantum Mater.* **5**, 85 (2020).
- [45] K. Guratinder, V. Tsurkan, L. Prodan, L. Keller, J. P. Embs, F. Juranyi, M. Medarde, C. Rüegg, and O. Zaharko, *Phys. Rev. B* **105**, 174423 (2022).
- [46] S. Gao, M. A. McGuire, Y. Liu, D. L. Abernathy, C. d. Cruz, M. Frontzek, M. B. Stone, and A. D. Christianson, *Phys. Rev. Lett.* **128**, 227201 (2022).
- [47] P. Ghosh, Y. Iqbal, T. Müller, R. T. Ponnaganti, R. Thomale, R. Narayanan, J. Reuther, M. J. P. Gingras, and H. O. Jeschke, *npj Quantum Mater.* **4**, 63 (2019).
- [48] J. M. Luttinger and L. Tisza, *Phys. Rev.* **70**, 954 (1946).
- [49] J. M. Luttinger, *Phys. Rev.* **81**, 1015 (1951).
- [50] U. Knauer and K. Knauer, *Algebraic Graph Theory: Morphisms, Monoids and Matrices* (De Gruyter, Berlin, 2019).
- [51] A. J. Kollár, M. Fitzpatrick, P. Sarnak, and A. A. Houck, *Commun. Math. Phys.* **376**, 1909 (2020).
- [52] A. Mielke, *J. Phys. A* **24**, L73 (1991).
- [53] H. Tasaki, *Phys. Rev. Lett.* **69**, 1608 (1992).
- [54] D.-S. Ma, Y. Xu, C. S. Chiu, N. Regnault, A. A. Houck, Z. Song, and B. A. Bernevig, *Phys. Rev. Lett.* **125**, 266403 (2020).
- [55] C. S. Chiu, A. N. Carroll, N. Regnault, and A. A. Houck, *Phys. Rev. Res.* **4**, 023063 (2022).
- [56] H. Nakai and C. Hotta, *Nat. Commun.* **13**, 579 (2022).
- [57] T. Mizoguchi, L. D. C. Jaubert, R. Moessner, and M. Udagawa, *Phys. Rev. B* **98**, 144446 (2018).
- [58] See Supplemental Material, which includes Refs. [59–70], at <http://link.aps.org/supplemental/10.1103/PhysRevLett.129.237202> for analytical solutions of the interaction matrices, discussions on the stability of the approximate spiral spin liquids, and experimental details.
- [59] F. L. Buessen, SpinMC.jl, <https://juliapackages.com/p/spinmc>.
- [60] K. Hukushima and K. Nemoto, *J. Phys. Soc. Jpn.* **65**, 1604 (1996).
- [61] A. S. Cameron, Y. V. Tymoshenko, P. Y. Portnichenko, J. Gavilano, V. Tsurkan, V. Felea, A. Loidl, S. Zherlitsyn, J. Wosnitzer, and D. S. Inosov, *J. Phys. Condens. Matter* **28**, 146001 (2016).
- [62] I. Jendrzewska, T. Groń, P. Kwapuliński, J. Kusz, E. Pietrasik, T. Goryczka, B. Sawicki, A. Ślebarski, M. Fijałkowski, J. Jampilek, and H. Duda, *Materials* **14**, 2749 (2021).
- [63] F. Ye, Y. Liu, R. Whitfield, R. Osborn, and S. Rosenkranz, *J. Appl. Crystallogr.* **51**, 315 (2018).
- [64] J. Rodriguez-Carvajal, *Physica (Amsterdam)* **192B**, 55 (1993).
- [65] O. Arnold *et al.*, *Nucl. Instrum. Methods Phys. Res., Sect. A* **764**, 156 (2014).
- [66] E. Farhi, Y. Debab, and P. Willendrup, *J. Neutron Res.* **17**, 5 (2014).
- [67] S. Calder, K. An, R. Boehler, C. R. Dela Cruz, M. D. Frontzek, M. Guthrie, B. Haberl, A. Huq, S. A. J. Kimber, J. Liu, J. J. Molaison, J. Neufeind, K. Page, A. M. dos Santos, K. M. Taddei, C. Tulk, and M. G. Tucker, *Rev. Sci. Instrum.* **89**, 092701 (2018).
- [68] S. Toth and B. Lake, *J. Phys. Condens. Matter* **27**, 166002 (2015).
- [69] M. I. Aroyo, J. M. Perez-Mato, D. Orobengoa, E. Tasci, G. de la Flor, and A. Kirov, *Bulg Chem Commun* **43**, 183 (2011).
- [70] C. C. Gu *et al.*, *Phys. Rev. Lett.* **120**, 147204 (2018).
- [71] J. G. Rau and M. J. P. Gingras, *Nat. Commun.* **7**, 12234 (2016).
- [72] M. Hering, H. Yan, and J. Reuther, *Phys. Rev. B* **104**, 064406 (2021).
- [73] D. Kiese, F. Ferrari, N. Astrakhantsev, N. Niggemann, P. Ghosh, T. Müller, R. Thomale, T. Neupert, J. Reuther, M. J. P. Gingras, S. Trebst, and Y. Iqbal, [arXiv:2206.00264](https://arxiv.org/abs/2206.00264).
- [74] M. Hirschberger, T. Nakajima, S. Gao, L. Peng, A. Kikkawa, T. Kurumaji, M. Kriener, Y. Yamasaki, H. Sagayama, H. Nakao, K. Ohishi, K. Kakurai, Y. Taguchi, X. Yu, T.-h. Arima, and Y. Tokura, *Nat. Commun.* **10**, 5831 (2019).
- [75] S. Gao, M. Hirschberger, O. Zaharko, T. Nakajima, T. Kurumaji, A. Kikkawa, J. Shiogai, A. Tsukazaki, S. Kimura, S. Awaji, Y. Taguchi, T.-h. Arima, and Y. Tokura, *Phys. Rev. B* **100**, 241115(R) (2019).
- [76] A. N. Yaresko, *Phys. Rev. B* **77**, 115106 (2008).
- [77] Y. V. Tymoshenko, Y. A. Onykiienko, T. Müller, R. Thomale, S. Rachel, A. S. Cameron, P. Y. Portnichenko, D. V. Efremov, V. Tsurkan, D. L. Abernathy, J. Ollivier, A. Schneidewind, A. Piovano, V. Felea, A. Loidl, and D. S. Inosov, *Phys. Rev. X* **7**, 041049 (2017).
- [78] J. Hemberger, H.-A. Krug von Nidda, V. Tsurkan, and A. Loidl, *Phys. Rev. Lett.* **98**, 147203 (2007).
- [79] F. Yokaichiya, A. Krimmel, V. Tsurkan, I. Margiolaki, P. Thompson, H. N. Bordallo, A. Buchsteiner, N. Stüßer, D. N. Argyriou, and A. Loidl, *Phys. Rev. B* **79**, 064423 (2009).
- [80] P. Zajdel, W.-Y. Li, W. van Beek, A. Lappas, A. Ziolkowska, S. Jaskiewicz, C. Stock, and M. A. Green, *Phys. Rev. B* **95**, 134401 (2017).
- [81] D. S. Inosov, Y. O. Onykiienko, Y. V. Tymoshenko, A. Akopyan, D. Shukla, N. Prasai, M. Doerr, D. Gorbunov, S. Zherlitsyn, D. J. Voneshen, M. Boehm, V. Tsurkan, V. Felea, A. Loidl, and J. L. Cohn, *Phys. Rev. B* **102**, 184431 (2020).
- [82] H. Duda, E. Maciążek, T. Groń, S. Mazur, A. W. Pacyna, A. Waśkowska, T. Mydlarz, and A. Gilewski, *Phys. Rev. B* **77**, 035207 (2008).
- [83] G. Pokharel, H. S. Arachchige, T. J. Williams, A. F. May, R. S. Fishman, G. Sala, S. Calder, G. Ehlers, D. S. Parker, T. Hong, A. Wildes, D. Mandrus, J. A. M. Paddison, and A. D. Christianson, *Phys. Rev. Lett.* **125**, 167201 (2020).
- [84] S.-H. Lee, W. Ratcliff, Q. Huang, T. H. Kim, and S.-W. Cheong, *Phys. Rev. B* **77**, 014405 (2008).
- [85] S. Gao *et al.*, *Phys. Rev. B* **97**, 134430 (2018).
- [86] V. Tsurkan, J. Hemberger, A. Krimmel, H.-A. Krug von Nidda, P. Lunkenheimer, S. Weber, V. Zestrea, and A. Loidl, *Phys. Rev. B* **73**, 224442 (2006).